On the Effect of Manganese on Grain Size Stability and Hardenability in Ultrafine-Grained Ferrite/Martensite Dual-Phase Steels

Marion Calcagnotto, Dirk Ponge & Dierk Raabe

Metallurgical and Materials Transactions A

ISSN 1073-5623
Volume 43
Number 1

Metall and Mat Trans A (2012) 43:37-46
DOI 10.1007/s11661-011-0828-3

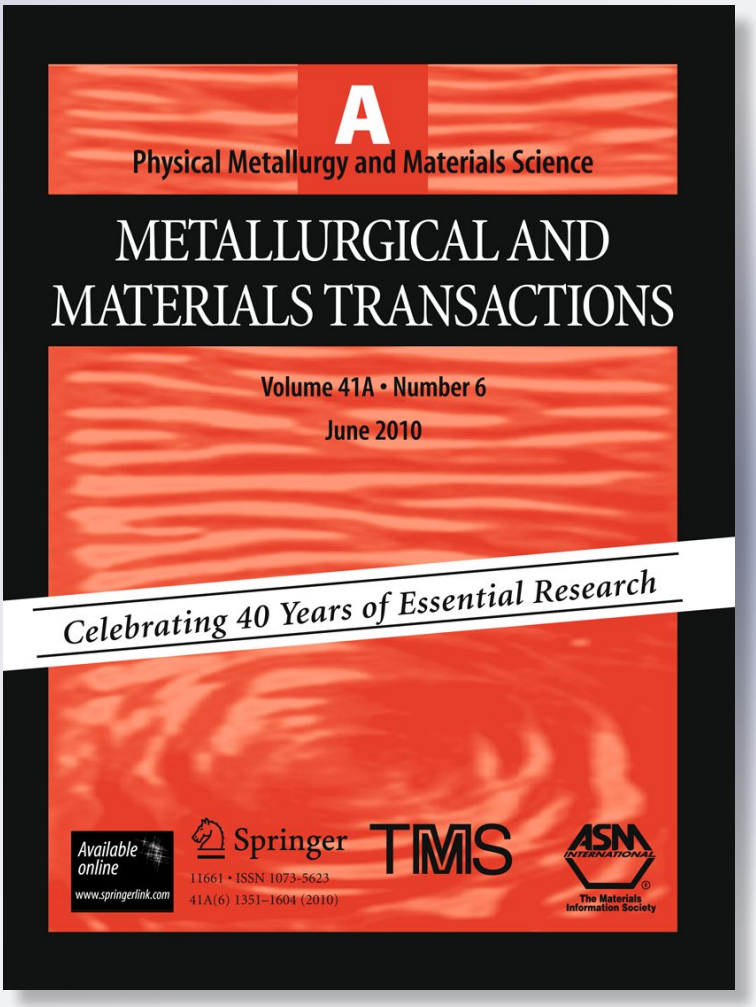

Springer

On the Effect of Manganese on Grain Size Stability and Hardenability in Ultrafine-Grained Ferrite/Martensite Dual-Phase Steels

MARION CALCAGNOTTO, DIRK PONGE, and DIERK RAABE

Two plain carbon steels with varying manganese content (0.87 wt pct and 1.63 wt pct) were refined to approximately 1 μm by large strain warm deformation and subsequently subjected to intercritical annealing to produce an ultrafine grained ferrite/martensite dual-phase steel. The influence of the Mn content on microstructure evolution is studied by scanning electron microscopy (SEM). The Mn distribution in ferrite and martensite is analyzed by high-resolution electron backscatter diffraction (EBSD) combined with energy dispersive X-ray spectroscopy (EDX). The experimental findings are supported by the calculated phase diagrams, equilibrium phase compositions, and the estimated diffusion distances using Thermo-Calc (Thermo-Calc Software, McMurray, PA) and Dictra (Thermo-Calc Software). Mn substantially enhances the grain size stability during intercritical annealing and the ability of austenite to undergo martensitic phase transformation. The first observation is explained in terms of the alteration of the phase transformation temperatures and the grain boundary mobility, while the second is a result of the Mn enrichment in cementite during large strain warm deformation, which is inherited by the newly formed austenite and increases its hardenability. The latter is the main reason why the ultrafine-grained material exhibits a hardenability that is comparable with the hardenability of the coarse-grained reference material.

DOI: 10.1007/s11661-011-0828-3

I. INTRODUCTION

FERRITE/martensite dual-phase (DP) steels are used for automotive applications as they combine high strength with good formability and weldability.[1] To meet the demands of improved crush resistance and reduced fuel consumption, further strengthening of DP steels is necessary. Grain refinement of DP steels offers a promising strengthening method as, unlike in other metallic materials, the increase in yield strength and tensile strength is not accompanied by a loss in strain hardenability or uniform elongation.[2–6] A variety of processing routes exists to achieve grain sizes of 1 μm and below.[7] Most studies focus on the production of ultrafine-grained (UFG) ferritic steels with finely dispersed cementite particles, whereas the number of studies on UFG DP steels is limited. Hence, a lack of systematic studies on the decisive parameters that control the microstructure evolution during the fabrication of UFG DP steels still exists. In particular, the effect of alloying elements on microstructure evolution has received little attention. Mukherjee *et al.*[8] studied the effect of molybdenum and niobium additions on the grain refinement process during deformation-induced ferrite transformation. Son *et al.*[3] investigated the effect of microalloying with vanadium on the mechanical properties of UFG DP steels fabricated by equal channel angular pressing (ECAP) and intercritical annealing. In a previous paper,[9] we demonstrated that a certain manganese content is crucial to obtain an UFG ferrite/martensite microstructure. This was explained with the lower transformation temperatures in case of the high-Mn steel and with the Mn enrichment in cementite that is inherited by austenite and enhances its hardenability. However, a detailed analysis of the phenomena involved, including thermodynamic simulations, has not been given so far and is the subject of the current article.

Austenite formation from conventional ferrite/pearlite starting microstructures and the Mn partitioning involved during intercritical annealing were studied in the past.[10–16] Reaustenitization basically takes place in three stages[10]: (1) rapid dissolution of pearlite; (2) slower growth of austenite into ferrite, the growth rate being controlled by carbon diffusion in austenite at high temperatures [~1123 K (~850 °C)] and by manganese diffusion in ferrite at low temperatures [~1023 K (~750 °C)]; and (3) slow final equilibration of ferrite and austenite at a rate that is controlled by manganese diffusion in austenite. Important factors that influence the phase transformation kinetics are the cementite morphology,[11,13] the grain size,[14] the heating rate,[15]

MARION CALCAGNOTTO, Researcher, formerly with Max-Planck-Institut für Eisenforschung GmbH, 40237 Düsseldorf, Germany, is now with Salzgitter Mannesmann Forschung GmbH, 38239 Salzgitter, Germany. DIRK PONGE, Group Leader, and DIERK RAABE, Director, are with Max-Planck-Institut für Eisenforschung GmbH. Contact e-mail: d.ponge@mpie.de
Manuscript submitted September 27, 2010.
Article published online August 12, 2011

and the preceding thermomechanical treatment of the material.[11,15,17] However, the main part of the studies was performed on relatively coarse-grained (CG) materials that were produced by conventional hot and/or cold deformation, exhibiting a ferrite/lamellar pearlite starting microstructure.

The hardenability defines the material's ability to suppress reconstructive transformation at a given cooling rate. A high hardenability is generally desired to reduce the sensitivity to industrial processing conditions. Furthermore, it was shown repeatedly that intermediate cooling rates yield better combinations of strength and ductility compared with rapidly quenched DP steels,[18–20] mainly because of the reduction of the interstitial carbon content in ferrite.[18] However, a systematic investigation on the hardenability of an UFG DP steel has not been performed so far.

In this study, two plain carbon steels with different Mn content are subjected to hot deformation, large strain warm deformation, and subsequent intercritical annealing to examine the influence of Mn on the grain refinement process and on the microstructure evolution during intercritical annealing. Mn as an alloying element is of special interest because it was shown to be highly beneficial for grain refinement.[21] Furthermore, it increases the hardenability and decreases the Ar_3 temperature (nonequilibrium ferrite formation start temperature during cooling). However, too high Mn contents promote segregation and undesired banded microstructures. The effect of the nominal Mn concentration on Mn partitioning is investigated by using high-resolution electron backscatter diffraction (EBSD) analysis combined with energy-dispersive X-ray spectroscopy (EDX), as well as thermodynamic equilibrium calculations using Thermo-Calc (Thermo-Calc Software, McMurray, PA)[22] and Dictra (Thermo-Calc Software).[23] The hardenability of the steel with higher Mn content is assessed by determining the critical cooling rate that allows full austenite-to-martensite phase transformation and compared with the hardenability of a CG reference material.

II. EXPERIMENTAL PROCEDURES

Two plain carbon manganese steels varying only in the Mn content (Table I) were produced by vacuum induction melting at the Max-Planck-Institut für Eisenforschung.

In this study, two different Mn contents were chosen to study the effect on microstructure evolution. For easy identification, the steel with lower Mn content will be called "15C steel" in the following, and the steel with higher Mn content "15CMn steel."

Samples (50 mm × 40 mm × 60 mm) were taken directly from the cast ingot. Thermomechanical processing was realized by use of a 2.5 MN hot deformation simulator.[24,25] This computer-controlled servohydraulic press allows simulating industrial rolling schedules by user-defined heating, deformation, and cooling setups. The UFG ferrite/cementite starting microstructure was produced by the consecutive steps of austenitization and hot deformation, large strain warm deformation in a four-pass flat compression test series (total strain: 1.6), and warm annealing. Grain refinement to a ferrite grain size of approximately 1 μm is achieved during large strain warm deformation because of grain subdivision and pronounced recovery of ferrite, as well as continuous fragmentation and spheroidization of cementite.[26] The final ferrite/martensite dual-phase steel is produced by intercritical annealing slightly above the Ac_1 temperature (nonequilibrium austenite formation start temperature during heating) to form the desired amount of austenite, followed by quenching to transform the austenite into martensite. Intercritical annealing was performed in a Bähr Dil805 A/D (Bähr-Thermoanalyse GmbH, Hüllhorst, Germany) quenching and deformation dilatometer using cylindrical samples with a diameter of 4 mm and a gauge length of 10 mm. The center of these specimens corresponds to the position in the warm-deformed sample where the local strain equals the nominal strain.[27] A CG reference material from the same laboratory melt was produced by the same austenitization and hot deformation treatment, yet this was followed by air cooling to room temperature. This CG ferrite/pearlite microstructure was subjected to identical intercritical annealing conditions that were established for the UFG materials. In this way, similar martensite volume fractions and martensite carbon contents are achieved.[5,6]

Samples for scanning electron microscopy (SEM) and EBSD investigations were prepared by standard mechanical grinding and polishing procedures, finishing with 3 min polishing with colloidal silica. The phase fractions were determined based on three SEM micrographs taken at a 3000 times magnification in case of the UFG material and at a 500 times magnification in case of the CG material. The point counting method was applied to assess the volume fraction of the phases. Here, a grid of 150 points was superimposed on each micrograph. The number of points covering martensite or bainite divided by the total number of points defines the respective phase fraction.

EBSD experiments were conducted using a JEOL JSM 6500F (JEOL Ltd, Tokyo, Japan) high-resolution, high-intensity SEM equipped with field-emission gun. The small beam diameter and its high brightness yield high-contrast Kikuchi patterns with a high signal to

Table I. Chemical Composition of the Steels Used, in wt pct

Steel	C	Mn	Si	Al	N	S	P	Fe
15C	0.16	0.87	0.27	0.037	0.0024	0.0034	0.0021	balance
15CMn	0.17	1.63	0.28	0.036	0.0025	0.0038	0.0021	balance

noise ratio, therefore allowing high spatial and angular resolution. A high-speed DigiView charge-coupled device (CCD) camera of EDAX-TSL (EDAX/TSL, Draper, UT) was used for pattern acquisition. The step size was 50 nm, which is close to the resolution limit of the system. The data were recorded and analyzed using the EDAX-TSL OIM Analysis (EDAX Inc., Mahwah, NJ) software package. Martensite was indexed as a body-centred-cubic phase and is distinguished from ferrite by its lower image quality (IQ) and confidence index, which is a result of the higher crystal lattice imperfection. The Mn distribution in ferrite and martensite was investigated semiquantitatively by the use of EDX attached to the SEM.

III. RESULTS

A. *Determination of the Intercritical Annealing Temperatures*

As it is known that Mn lowers the $\alpha \rightarrow \gamma$ (ferrite to austenite) transformation start temperature, the intercritical annealing temperature for the 15C and the 15CMn alloys (Table II) must be different to obtain the same martensite fraction.

To define a suitable intercritical annealing temperature for both chemical compositions and to gain insight into the influence of the Mn content on phase transformation in the current materials, the phase diagrams were calculated to determine the equilibrium temperatures, and dilatometer tests were performed to identify the phase transformation start and finish temperatures under experimental conditions.

The equilibrium phase diagrams and the respective phase transformation start and finish temperatures were calculated using Thermo-Calc,[21] version TCCR, database TCFE5 (Figure 1). Comparing the phase diagrams of the 15C steel (Figure 1(a)) and the 15CMn (Figure 1(b)), it is evident that Mn (as an austenite stabilizing alloying element) reduces the equilibrium austenite formation start (Ae_1) and finish (Ae_3) temperatures. The respective values are given in Table II.

The $\alpha + \gamma + \text{cem}$ (ferrite + austenite + cementite) three-phase field is broadened with increasing Mn content. Therefore, cementite is replaced completely by austenite at 985 K (712 °C) in the 15C steel and at 969 K (696 °C) in the 15CMn steel. The equilibrium temperature at which the microstructure consists of 30 vol pct austenite and 70 vol pct ferrite is 1017 K (744 °C) in the 15C steel and 986 K (713 °C) in the 15CMn steel. As Mn reduces the carbon solubility in ferrite, the cementite fraction at room temperature is slightly higher in the 15CMn steel than in the 15C steel (2.37 pct compared with 2.5 pct). It has to be noted that the stochiometric cementite phase (Fe_3C) is replaced because of the addition of Mn by Fe-Mn carbides of various stochiometries, *e.g.,* $(Fe,Mn)_7C_3$. Therefore, the general term "carbide" would be more appropriate to describe the current microstructure. However, the term

Table II. Comparison of the Equilibrium and Experimental Phase Transformation Start and Finish Temperatures Obtained from the Phase Diagrams (Ae_1 and Ae_3) and the Dilatometer Tests (Ac_1 and Ac_3)

	Equilibrium			Experimental	
Steel	Ae_1 [K (°C)]	Ae_3 [K (°C)]	T [K (°C)] at 30 vol pct γ	Ac_1 [K (°C)]	Ac_3 [K (°C)]
15C	977 (704)	1109 (836)	1017 (744)	1006 (733)	1118 (845)
15CMn	952 (679)	1083 (810)	986 (713)	994 (721)	1108 (835)

γ: Austenite.

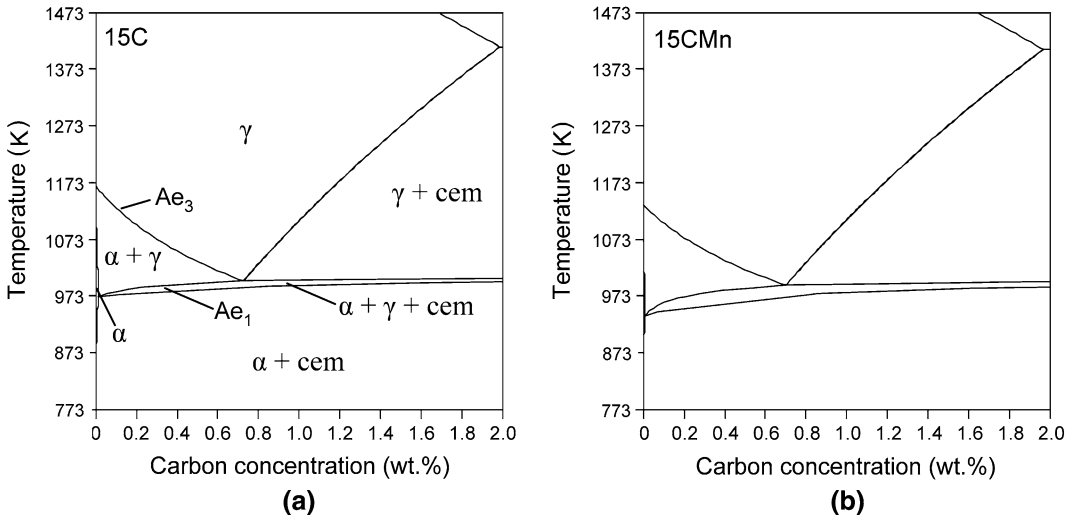

Fig. 1—Equilibrium phase diagrams for the 15C (*a*) and the 15CMn (*b*) steel. As an austenite stabilizing element, Mn lowers the phase transformation start (Ae_1) and finish (Ae_3) temperatures. Moreover, it broadens the ferrite + austenite + cementite ($\alpha + \gamma + \text{cem}$) three-phase field.

"cementite" is used conventionally in the literature because the different carbides cannot be distinguished in micrographs. Therefore, the term "cementite" is used in this study. The equilibrium calculations using Thermo-Calc and Dictra[22] were performed using cementite as the only carbide phase to obtain results that can be compared directly with the microstructure.

To determine the intercritical annealing range under experimental conditions, several samples of both materials were heated at a rate of 1 K/s to 1173 K (900 °C), held for 2 minutes, and then cooled to room temperature. The Ac_1 and Ac_3 temperatures (nonequilibrium austenite formation start and finish temperatures during heating) were determined from the change in length *vs* temperature curves (Figure 2(a)). In the first stage, the sample length increases linearly with temperature as a result of thermal expansion. As the $\alpha + \text{cem} \rightarrow \gamma$ phase transformation is accompanied by a volume decrease because of the closer packed face-centered cubic crystal lattice of austenite, the onset of phase transformation (Ac_1) can be read from the curves as the first deviation from linearity. The transformation finish temperature (Ac_3) is read from the point where linearity is reestablished. It is well known that the austenite formation takes place in two steps: (1) rapid dissolution of cementite in the $\alpha + \gamma + \text{cem}$ three-phase field and (2) slower growth of austenite at the expense of ferrite in the $\alpha + \gamma$ two-phase field. The transition from step (1) to step (2) is reflected in the curves by the change in slope between the Ac_1 and Ac_3 temperatures.

The results of several dilatometer tests are shown in Figure 2(b). For a comparison, the equilibrium Ae_1 and Ae_3 temperatures were calculated for a range of Mn contents using Thermo-Calc. It can be observed that the equilibrium and experimental values are in good agreement and that they show the same decreasing tendency with increasing Mn content. However, the mismatch between calculated and measured values is higher in the case of the 15CMn steel. A possible explanation for this discrepancy is that Mn decreases the carbon activity. As the phase transformation is controlled mainly by carbon diffusion, the reduced carbon activity retards the phase transformation. The mismatch is also higher for the Ac_1 than for the Ac_3 temperatures in both materials. The reason for the delay of the phase transformation onset is possibly that a certain overheating is necessary under nonequilibrium conditions to initiate austenite nucleation.

Based on these findings, the intercritical annealing temperature was set at 1023 K (750 °C) for the 15C steel and to 1003 K (730 °C) for the 15CMn steel. At these temperatures, a cementite-free microstructure containing 25–30 vol pct of austenite is expected.

B. *Microstructures Before and After Intercritical Annealing*

Both steels were heated at a rate of 20 K/s to the intercritical annealing temperature [1023 K (750 °C) for the 15C and 1003 K (730 °C) for the 15CMn steel, respectively], held for 3 minutes, and quenched with hydrogen gas to room temperature at a cooling rate of – 140 K/s. It was shown previously,[9] that the heating rate does not exert a considerable effect on microstructure evolution. Therefore, the faster heating applied in this party of the study is considered to be insignificant. Figure 3 shows the microstructures before and after intercritical annealing. In the left column, the UFG ferrite/cementite (F/C) steels fabricated by large strain warm deformation and annealing are presented, and the same samples after subsequent intercritical annealing are given in the right column.

The UFG-F/C microstructure is similar in both materials, yet in the 15C steel, the ferrite grain size is slightly larger and the cementite particles are somewhat larger and thus less numerous. It is obvious that during intercritical annealing, phase transformation has happened in both materials. However, the austenite in the 15C steel transformed into martensite only partially. The remaining austenite has undergone phase transfor-

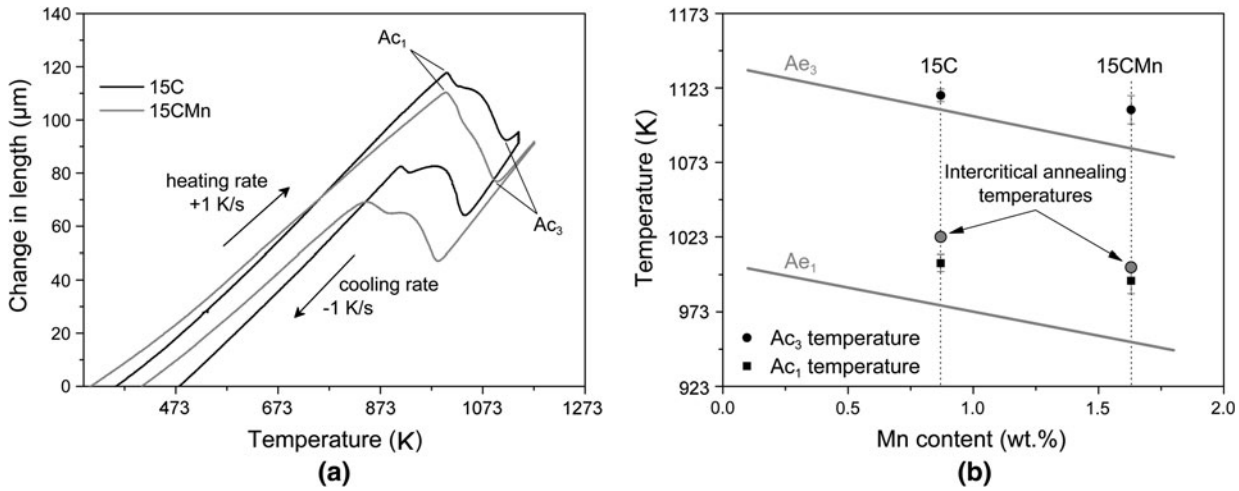

Fig. 2—Results of the dilatometer tests. (*a*) The phase transformation start (Ac_1) and finish (Ac_3) temperatures are read from the change in length versus temperature curves. (*b*) The results of several dilatometer tests are compared with the equilibrium temperatures (Ae_1 and Ae_3), and a suitable intercritical annealing temperature is defined.

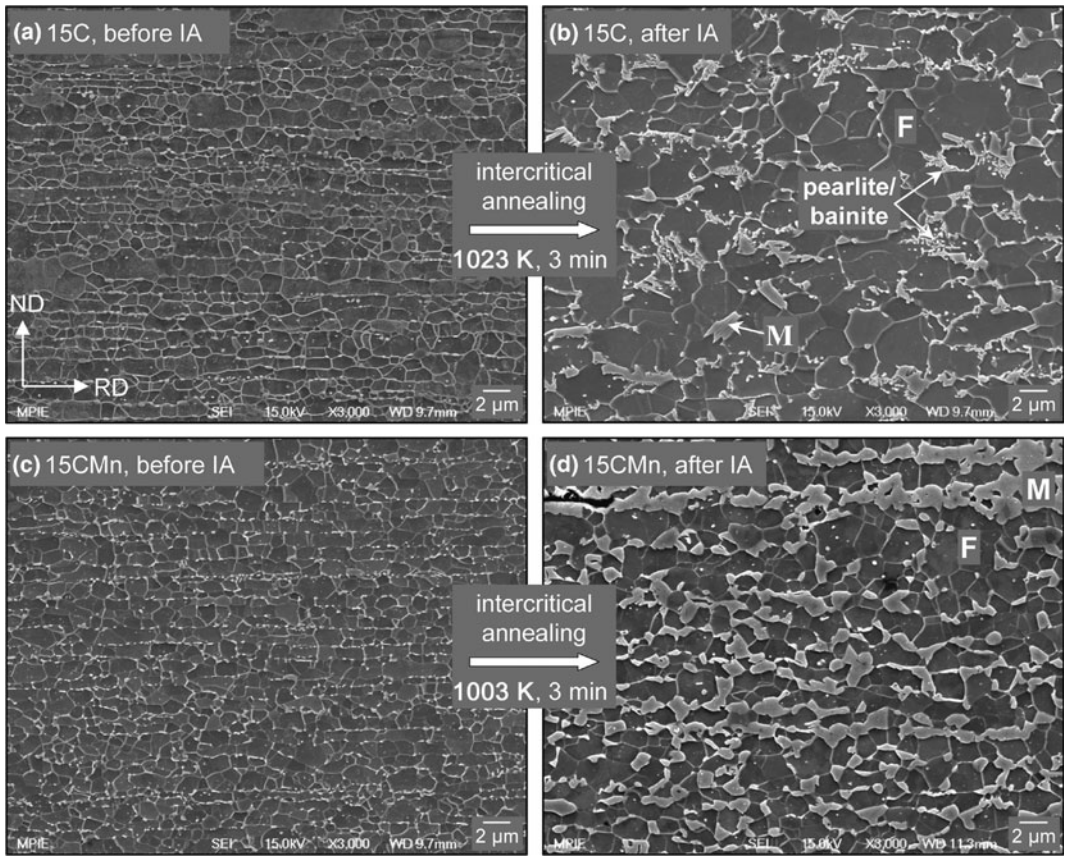

Fig. 3—Effects of chemical composition on microstructure evolution during intercritical annealing (IA) performed in a dilatometer. The ultra-fine-grained ferrite/cementite microstructure of the 15C steel (*a*) transforms into a fine-grained ferrite (F) matrix with martensite (M) and pearlitic/bainitic areas (*b*), whereas the 15CMn steel (*c*) exhibits the desired UFG ferrite/martensite dual-phase structure after intercritical annealing (*d*). Indication of rolling direction (RD) and normal direction (ND) counts for all images.

mation into bainite and/or pearlite. Furthermore, considerable grain growth has happened in the 15C steel.

In the 15CMn steel, the whole austenite has undergone displacive transformation into martensite, except minor amounts of retained austenite that are not detectable in the SEM images. The ferrite grain size (mean linear intercept length) was 1.2 μm and the martensite volume fraction 24.3 pct. For more detailed quantification of the microstructure characteristics, the reader is referred to a paper recently submitted by our group.[28] Hence, the desired microstructure is only obtainable when a certain Mn content is added. As the only difference between the materials is the Mn content, the reason for the unlike microstructure evolution must be found in the Mn distribution.

C. *Mn Distribution Studied by EDX*

The Mn partitioning between the phases can be visualized by high-resolution EBSD maps combined with EDX analysis. Figure 4 shows the grayscale IQ maps and the respective EDX maps of Mn of the 15C steel (Figure 4(a), micrograph in Figure 3(b)), and the 15CMn steel (Figure 4(b), micrograph in Figure 3(d)). Martensite is characterized by a lower IQ value because of the larger lattice distortions, thus appearing dark gray in the IQ map. Retained austenite is marked in white on the IQ maps. One can observe that the martensite islands are subdivided into blocks. Retained austenite is isolated partly in the ferrite matrix and occurs partly within the martensite islands.

The EDX maps show the Mn distribution in a semiquantitative way. The scaling is normalized to 15 to 90 pct of the maximum Mn X-ray counts. For a more convenient comparison with the respective IQ map, the grain boundaries are superimposed. In the 15C steel, a slight enrichment in Mn is observed in some bainitic/martensitic areas (encircled). However, the overall distribution of Mn is homogeneous. In contrast, Mn segregation in the 15CMn steel (Figure 4(b)) parallel to the rolling direction is obvious. Martensite is situated mostly in the areas of high Mn concentration. In contrast, the ferrite matrix is depleted in Mn.

It is well known that the nucleation of austenite from ferrite/cementite structures starts at the interface between both phases.[10,29] Therefore, the Mn-enrichment in cementite is of particular importance for the intercritical annealing applied in this study. As one can observe from Figure 4(b), both martensite and retained austenite are enriched in Mn in comparison with the ferrite matrix. In particular, small martensite islands that are located along the rolling direction inherit the

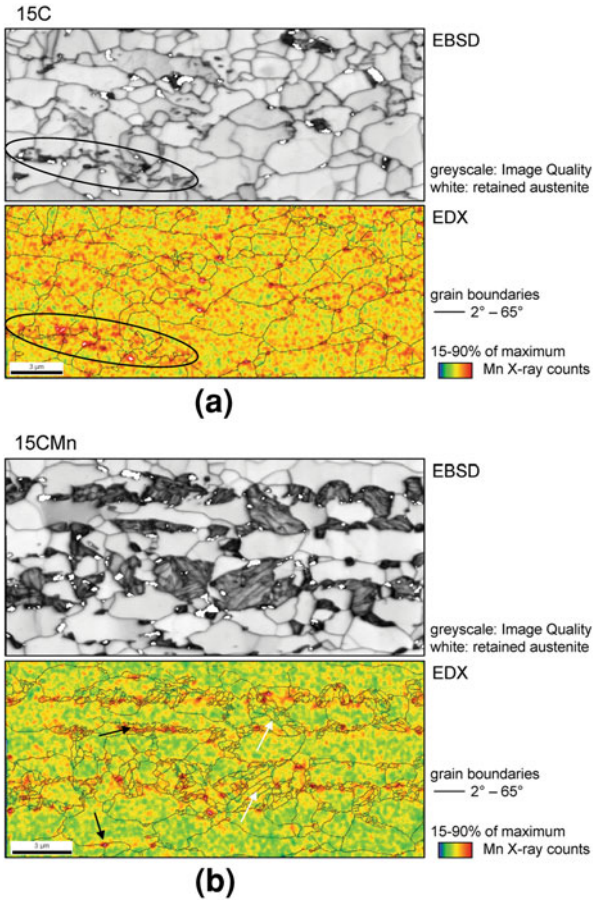

Fig. 4—High-resolution electron backscatter diffraction (EBSD) scans combined with energy dispersive X-ray spectroscopy (EDX) analysis of the 15C (*a*) and the 15CMn steel (*b*). The grayscale images show the Image Quality maps. The position of retained austenite is superimposed in white. The EDX maps are normalized for 15–19 pct of the maximum EDX counts for better visualization of the Mn distribution. Rolling direction is horizontal, and normal direction is vertical.

high Mn content from the cementite and the segregation pattern (black arrows). Some larger martensite islands do not show considerable Mn enrichment (white arrows).

D. *Hardenability of the 15CMn Steel and its Coarse-Grained Counterpart*

The hardenability of the 15CMn steel was assessed by applying different cooling rates after intercritical annealing and observation of the obtained microstructure to determine the minimum cooling rate that allows complete austenite-to-martensite phase transformation. As the 15C steel does not show full martensitic phase transformation even at the highest possible cooling rate, this part of the study was only performed with the 15CMn material. The samples were heated to 1003 K (730 °C), held for 1 minute, and then cooled at rates between –140 K/s and –10 K/s. After slow cooling, phase equilibrium is shifted to lower temperatures and consequently to lower austenite fractions with a higher carbon content. We found that slower cooling provides enough time for ferrite to grow into austenite after cooling. Thus, the lower the cooling rate (*i.e.,* the longer the cooling time between intercritical annealing temperature and room temperature), the lower the martensite fraction and the larger the ferrite grain size. Slower cooling impedes martensite banding because of the epitaxial growth of ferrite. At a cooling rate of –20 K/s, minor parts of the UFG microstructure consist of bainite instead of martensite, so that this cooling rate is considered to be the critical cooling rate.

The same intercritical annealing conditions were applied to the CG counterpart having the same chemical composition and martensite volume fraction[5,6] in order to address the question to what extent the grain refinement process affects the hardenability of the steel. The bainite fraction was determined in order to assess the decreasing ability of the material to undergo reconstructive transformation with decreasing cooling rate. Bainite was determined manually on the basis of SEM micrographs. No differentiation was made between bainite and pearlite because of the similar morphology. Two micrographs of the materials cooled at –10 K/s are shown in Figure 5. Note the different magnifications of the images. One can observe that the main part of the UFG DP steel (Figure 5(a)) consists of martensite, whereas some austenite grains obviously decomposed into bainite (arrows). In contrast, the main fraction of the austenite for the CG material (Figure 5(b)) has undergone phase transformation into bainite and/or pearlite. Only small areas consist of martensite (arrows).

The bainite fraction as a function of grain size and cooling rate is shown in Figure 6. Additionally, the bainite fraction divided by the total second phase fraction (bainite + martensite) is illustrated. On the *x* axis, the cooling time between the intercritical annealing temperature and 773 K (500 °C) is shown, as this is the decisive parameter for displacive transformation. At the shortest cooling time (cooling rate –140 K/s), all austenite is transformed into martensite. Bainite formation is detectable in both materials at a cooling rate of –50 K/s, yet the volume fraction is low (~1 vol pct). Further decreasing the cooling rate leads to a substantial increase in bainite fraction in both materials. However, the rate of increase is much higher in the CG material than in the UFG material. For example, at a cooling rate of –15 K/s, the UFG material consists of 8.2 vol pct bainite, whereas the CG material contains 19.3 vol pct bainite. At this point, bainite makes up 42 pct of the total second phase fraction in the UFG DP steel, and even 77 pct in the CG counterpart. At even lower cooling rates, the bainite fraction in the UFG steel tends to stabilize, whereas it is increased to 24 vol pct in the CG material.

IV. DISCUSSION

A. *Effect of Mn on Grain Size Stability*

When comparing the microstructure after intercritical annealing of the 15C steel (0.87 wt pct Mn) with the 15CMn steel (1.63 wt pct Mn) in Figure 3, the importance of a critical amount of Mn to suppress grain

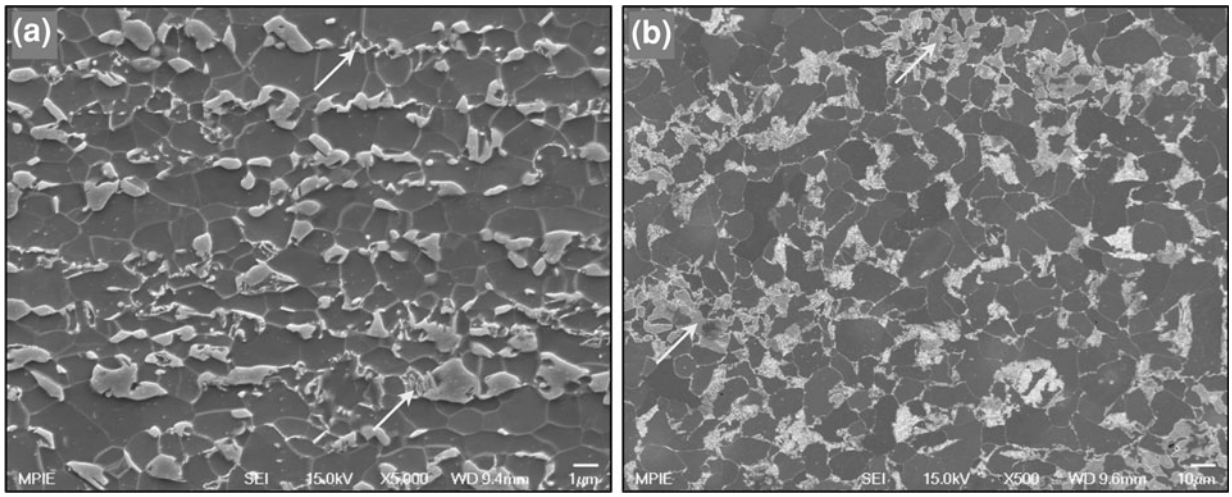

Fig. 5—Typical micrographs of the ultrafine-grained (*a*) and the coarse-grained (*b*) dual-phase steels (composition 15CMn), which were subjected to intercritical annealing at 1003 K (730 °C) for 1 min, followed by cooling at a rate of –10 K/s. Note the different magnification in the two images. Rolling direction is horizontal, and the normal direction is vertical.

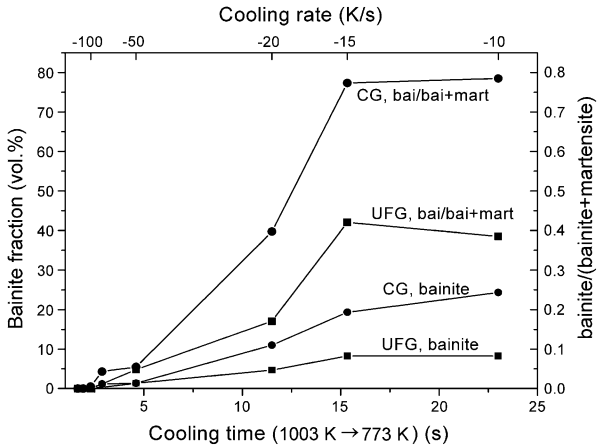

Fig. 6—Influence of cooling rate on bainite (and/or pearlite) fraction showing the higher hardenability of the ultrafine-grained (UFG) material compared with the coarse-grained (CG) counterpart.

growth is obvious. Mn contributes to the grain size stability of the UFG material in several ways.

The most beneficial effect of Mn is that it decreases the Ac_1 temperature. Therefore, it is possible to achieve the same amount of austenite at lower temperatures. For example, the equilibrium intercritical annealing temperature to achieve 30 vol pct austenite is 1017 K (744 °C) in the 15C steel (Figure 7) but only 986 K (713 °C) in the 15CMn steel. In the experiment, the intercritical annealing temperature in the 15C steel was 1023 K (750 °C), whereas it was 1003 K (730 °C) in the 15CMn steel. Annealing at lower temperatures means slower kinetics of grain growth.

The second effect of Mn is that it broadens the $\alpha + \gamma + \text{cem}$ three-phase field (Figure 1). Therefore, most of the phase transformation in the 15CMn steel occurs within the three-phase field. This can be best visualized by plotting the equilibrium phase fractions as a function of temperature (Figure 7). To achieve an austenite volume fraction of 30 pct, a greater temperature increase after complete dissolution of cementite is necessary in the 15C steel than in the 15CMn steel. It is known that grain growth is inhibited strongly in the three-phase field because of the coexistence of cementite and austenite. Therefore, grain growth is suppressed longer in the 15CMn steel than in the 15C steel. Although equilibrium conditions are not achieved under the current experimental conditions, it is likely that the longer intercritical annealing above the three-phase field contributes to grain growth in the 15C steel.

Third, the addition of Mn leads to a finer distribution of cementite in the initial microstructure (Figure 3). Song *et al.*[21] explain this effect by the enrichment of Mn in cementite that occurs during large strain warm deformation and warm annealing because of the introduction of dislocations, vacancies, and high-angle grain boundaries during dynamic and static recovery. Cementite is then replaced by Mn-Fe carbides that are characterized by a higher stability.[30] The higher stability of the Fe-Mn carbides makes them more resistant to Ostwald ripening and therefore leads to a finer distribution of these particles. Hence, the greater number of cementite particles in the 15CMn steel exerts a more effective pinning effect on the grain boundaries, therefore suppressing grain growth. The efficiency of boundary pinning during intercritical annealing by spheroidized cementite has been demonstrated by Garcia and DeArdo[11] on the basis of a low alloy steel containing different carbon contents. The authors studied the austenite formation from spheroidized cementite in a ferrite matrix and found that extensive grain growth during intercritical annealing occurs only in case of the lowest carbon content.

Furthermore, Mn in solid solution exerts a solute drag effect and thus reduces the grain boundary mobility.[31]

B. *Effect of Mn on Hardenability*

Primarily, hardenability is a function of the carbon content in austenite. However, Mn was found to also

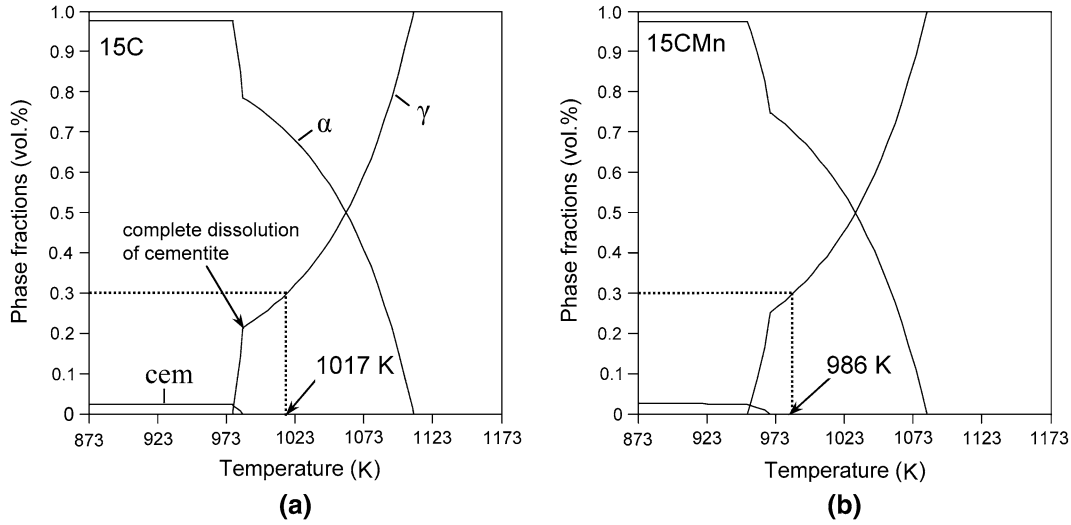

Fig. 7—Equilibrium phase volume fractions as a function of temperature in the 15C (*a*) and in the 15CMn steel (*b*): α: ferrite, γ: austenite, cem: cementite.

increase hardenability substantially.[32] Being an austenite-stabilizing element, Mn partitions preferentially to austenite and increases its hardenability, *i.e.,* it retards proeutectoid ferrite, pearlite, and bainite formation. Moreover, Mn increases the carbon solubility in austenite, which enhances its hardenability. Hence, Mn lowers the critical cooling rate for martensite formation. For this reason, the low hardenability of the 15C is surprising. Even the fastest quench at –140 K/s was not enough to transform all austenite into martensite, although the Mn content (0.87 wt pct) is not marginal. Hence, it is anticipated that not only the nominal Mn content of the material is decisive to allow a good hardenability but also the processing route. It was shown that the Mn enrichment in cementite, which takes place during large-strain warm deformation and warm annealing,[21] is inherited by the newly formed austenite during intercritical annealing and in the following by the martensite (Figure 4). This is enabled by the low diffusion coefficient of Mn in austenite. The diffusion coefficient D of Mn in austenite at 1003 K (730 °C) was estimated using Dictra, applying the mobility database v.2.[22] It is $4.2 \times 10^{-19} m^2 s^{-1}$, which is close to the values reported by Atkinson *et al.*[12] and by Speich *et al.*[10], who studied similar temperatures and compositions. The diffusion distance l can be estimated from conventional random walk kinetics as

$$l = 2 \cdot \sqrt{D \cdot t_{IA}} \qquad [1]$$

Hence, within the intercritical annealing time t_{IA} of 1 minute, the diffusion distance of Mn in austenite is 0.01 μm. This explains the observation in Figure 4, that large martensite islands are not fully enriched in Mn. Mn is preserved in the location of the former cementite particle and austenite growth is controlled by the diffusion of carbon which is commonly expected at 1003 K (730 °C).[29] It is followed that the Mn enrichment in the austenite islands controls the hardenability

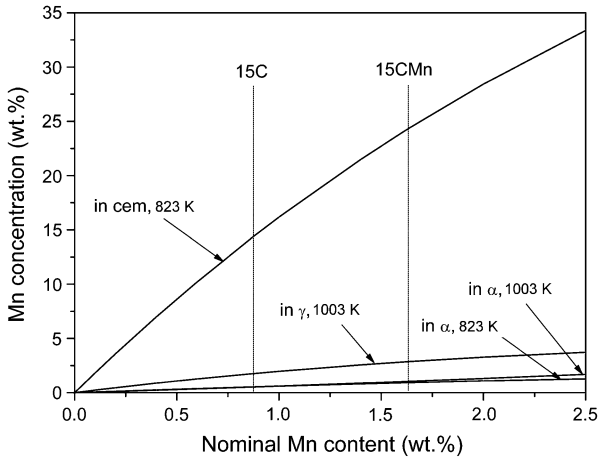

Fig. 8—Equilibrium Mn enrichment in cementite (cem), austenite (γ), and ferrite (α) as a function of nominal Mn content revealing the drastic increase in Mn enrichment in cementite by increasing the Mn content from 0.87 to 1.63 wt pct.

of the material. In both the 15C and the 15CMn steel, Mn enrichment takes place during large strain warm deformation. Yet, Mn enrichment is more pronounced in the 15CMn steel as is revealed by the combined EBSD and EDX maps. Hence, the lower nominal Mn content in the 15C does not yield enough Mn enrichment in cementite so as to increase the hardenability of the newly formed austenite successively.

Examining the equilibrium values of Mn in cementite helps to clarify this observation. In Figure 8, the Mn content in cementite, ferrite, and austenite is plotted as a function of the nominal Mn concentration in the material. Increasing the Mn content from 0.87 wt pct (15C) to 1.63 wt pct (15CMn) increases the equilibrium Mn concentration in cementite from 14 pct to 24 pct at the deformation temperature [823 K (550 °C)]. In contrast, the Mn concentration in ferrite is much lower and

does not change remarkably with increasing nominal Mn concentration. Although full equilibrium is not reached during processing, the remarkable increase of Mn content in cementite as a result of a higher nominal Mn concentration was shown experimentally.[21] At the intercritical annealing temperature of 1003 K (730 °C), the equilibrium values in austenite are naturally much lower than in cementite. As the austenite fraction at 1003 K (730 °C) is much higher than the cementite fraction at 823 K (550 °C), Mn is diluted. However, the dilution is not accomplished within the short intercritical annealing time given due to the low diffusion coefficient of Mn (see preceding text). Therefore, one can conclude that the higher hardenability of the 15CMn steel is a consequence of the Mn enrichment in cementite during large-strain warm deformation. The lower nominal Mn content in the 15C steel does not result in Mn partitioning that is high enough to ensure a Mn content of the reversed austenite that allows full martensitic transformation.

C. *Effect of Grain Refinement on Hardenability*

The hardenability of the 15CMn steel is considerable not only with respect to the absence of additional alloying elements like Mo or Cr but also with respect to its small grain size. In general, a CG microstructure exhibits a higher hardenability than a fine-grained microstructure. This is because austenite decomposition starts at grain boundaries. Therefore, the lower grain boundary fraction in coarser microstructures delays austenite decomposition because of the reduction of potential pearlite or bainite nucleation sites. However, the critical cooling rate of the CG (ferrite grain size 12.4 μm) and the UFG steel (ferrite grain size 1.2 μm) were found to be nearly identical (between –50 K/s and –20 K/s, Figure 6). As the nominal Mn content is the same in the materials, it must be the processing route that determines the hardenability. The CG material has undergone a one-pass hot rolling step, which is performed above the Ar_3 temperature and thus does not lead to Mn enrichment in pearlite. In contrast, warm deformation to produce the UFG microstructure is applied below Ac_1 temperature and leads to considerable Mn enrichment in cementite. Therefore, it is concluded that the detrimental effect of the high-grain-boundary density is balanced by the beneficial effect of a higher Mn content in cementite that is inherited by austenite, giving rise to a comparable critical cooling rate in the CG and the UFG material.

It was found that with decreasing cooling rate the bainite fraction increases at a much higher rate in the CG material than in the UFG material. That means, the ability to undergo martensitic transformation is maintained more successfully in the UFG material at slower cooling. At slow cooling, ferrite grows at the expense of austenite, thereby rejecting carbon into austenite. This process is facilitated when diffusion distances are short. Therefore, carbon enrichment in the austenite during slow cooling is much more effective in the UFG steel, thus leading to a higher hardenability of the remaining austenite. This explains that even at the lowest tested cooling rate of –10 K/s only approximately 40 pct of the total second phase fraction is made up of bainite in the UFG material, whereas bainite constitutes around 78 pct of the second phase fraction in the CG steel.

V. CONCLUSIONS

Two UFG plain C-Mn steels varying only in the Mn content (15C: 0.87 wt pct Mn, 15CMn: 1.63 wt pct Mn) were subjected to intercritical annealing to study the differences in the microstructure evolution. The hardenability of the 15CMn steel was determined and compared to its CG counterpart. The main conclusions are as follows:

1. A certain Mn content is necessary to avoid grain growth during intercritical annealing and to ensure sufficient hardenability to transform all austenite into martensite upon cooling.
2. Mn enhances the grain size stability by (1) lowering the Ac_1 temperature and thus, the intercritical annealing temperature; (2) broadening the $\alpha + \gamma + \text{cem}$ three-phase field in which grain growth is inhibited; (3) refining cementite, which causes a more efficient pinning effect; and (4) reducing the grain boundary mobility by solute drag.
3. The hardenability is controlled by Mn partitioning between ferrite and cementite, which is established during large strain warm deformation. The high Mn concentration in cementite is preserved in austenite and increases its hardenability.
4. The hardenability of the UFG DP steel (15CMn) is comparable to its CG counterpart in terms of the critical cooling rate (–20 K/s to –50 K/s). The detrimental effect of a high grain boundary fraction is compensated for by the higher Mn concentration in austenite in the UFG steel.
5. The ability to accomplish the martensitic phase transformation at decreasing cooling rates is higher in the UFG material than in the CG material because of the more effective carbon enrichment in austenite during cooling.

REFERENCES

1. K.P. Imlau and T. Heller: *Steel Res. Int*., 2007, vol. 78, pp. 180–84.
2. Z.H. Jiang, Z.Z. Guan, and J.S. Lian: *Mater. Sci. Eng. A*, 1995, vol. 190, pp. 55–64.
3. Y.I. Son, Y.K. Lee, K.T. Park, C.S. Lee, and D.H. Shin: *Acta Mater*., 2005, vol. 53, pp. 3125–34.
4. M. Delincé, Y. Brechet, J.D. Embury, M.G.D. Geers, P.J. Jacques, and T. Pardoen: *Acta Mater*., 2007, vol. 55, pp. 2337–50.
5. M. Calcagnotto, D. Ponge, and D. Raabe: *Mater. Sci. Eng. A*, 2010, vol. 527, pp. 7832–40.
6. M. Calcagnotto, Y. Adachi, D. Ponge, and D. Raabe: *Acta Mater*., 2010, vol. 59, pp. 2738–46.
7. R. Song, D. Ponge, D. Raabe, J.G. Speer, and D.K. Matlock: *Mater. Sci. Eng. A*, 2006, vol. 441, pp. 1–17.
8. K. Mukherjee, S.S. Hazra, and M. Militzer: *Metall. Mater. Trans. A*, 2009, vol. 40A, pp. 2145–59.
9. M. Calcagnotto, D. Ponge, and D. Raabe: *ISIJ Int*., 2008, vol. 48, pp. 1096–1101.

10. G.R. Speich, V.A. Demarest, and R.L. Miller: *Metall. Trans. A*, 1981, vol. 12A, pp. 1419–28.
11. C.I. Garcia and A.J. DeArdo: *Metall. Trans. A*, 1981, vol. 12A, pp. 521–30.
12. C. Atkinson, T. Akbay, and R.C. Reed: *Acta Metall. Mater.*, 1995, vol. 43, pp. 2013–31.
13. D.V. Shtansky, K. Nakai, and Y. Ohmori: *Z. Metallkd.*, 1999, vol. 90, pp. 25–37.
14. S.J. Sun and M. Pugh: *Mater. Sci. Eng. A*, 2000, vol. 276, pp. 167–74.
15. J. Huang, W.J. Poole, and M. Militzer: *Metall. Mater. Trans. A*, 2004, vol. 35A, pp. 3363–75.
16. N. Maruyama, T. Ogawa, and M. Takahashi: *Mater. Sci. Forum*, 2007, vols. 558-9, pp. 247–52.
17. Y.I. Son, Y.K. Lee, and K.T. Park: *Metall. Mater. Trans. A*, 2006, vol. 37A, pp. 3161–64.
18. S. Hayami, T. Furukawa, H. Gondoh, and H. Takechi: *Formable HSLA and Dual-Phase Steels*, Ed. A.D. Davenport, TMS, New York, NY, 1979, pp. 167–80.
19. D.K. Matlock, G. Krauss, L.F. Ramos, and G.S. Huppi: *Structure and Properties of Dual-Phase Steels*, Eds. R.A. Kot and J.W. Morris, TMS, New York, NY, 1979, pp. 62–90.
20. S.S. Hansen and R.R. Pradhan: *Fundamentals of Dual-Phase Steels*, Eds. R.A. Kot and B.L. Bramfitt, TMS, New York, NY, 1981, pp. 113–44.
21. R. Song, D. Ponge, and D. Raabe: *ISIJ Int.*, 2005, vol. 45, pp. 1721–26.
22. B. Jansson, M. Schalin, M. Selleby, and B. Sundman: *Computer Software in Chemical and Extractive Metallurgy*, Eds. C.W. Bale and G.A. Irons, The Metallurgical Society of CIM, Quebec, Canada, 1993, pp. 57–71.
23. A. Borgenstam, A. Engstrom, L. Hoglund, and J. Agren: *J. Phase Equilib.*, 2000, vol. 21, pp. 269–80.
24. O. Pawelski and R. Kaspar: *Materialprüfung*, 1988, vol. 30, pp. 357–60.
25. R. Kaspar and O. Pawelski: *Materialprüfung*, 1989, vol. 31, pp. 14–16.
26. R. Song, D. Ponge, D. Raabe, and R. Kaspar: *Acta Mater.*, 2005, vol. 53, pp. 845–58.
27. J.S. Distl, A. Streißelberger, R. Kaspar, and U. Zeislmair: *Materialprüfung*, 1985, vol. 27, pp. 131–35.
28. M. Calcagnotto, D. Ponge, and D. Raabe: *ISIJ Int.*, 2011, In press.
29. M. Hillert, K. Nilsson, and L.E. Torndahl: *J. Iron Steel Inst.*, 1971, vol. 209, pp. 49–66.
30. Y.C. Zhang and D.M. Schleich: *J. Solid State Chem.*, 1994, vol. 110, pp. 270–73.
31. D.A. Porter, K.E. Easterling, and M.Y. Sherif: *Phase Transformations in Metals and Alloys*, CRC Press, Boca Raton, FL, 2009.
32. R.A. Grange: *Metall. Trans.*, 1973, vol. 4, pp. 2231–44.